Static Stability in the Extratropical Tropopause Region

VOLKMAR WIRTH

University of Mainz, Mainz, Germany

(Manuscript received 18 July 2002, in final form 8 November 2002)

ABSTRACT

Idealized axisymmetric anomalies of potential vorticity (PV) on a midlatitude f plane and their related response in terms of balanced wind and temperature are investigated with special focus on the static stability in the tropopause region. The PV anomalies are specified such that they can be interpreted as the result of conservative advection in the tropopause region across the gradients of a prescribed background atmosphere with piecewise constant buoyancy frequency squared N^2. Related cyclones and anticyclones are treated identically except for the sign of the tropopause potential temperature anomaly. Composite profiles of N^2 are computed, for which the thermal tropopause is used as a common reference level and where the number of cyclones in the composite equals the number of anticyclones. One obtains a pronounced peak of N^2 just above the tropopause and slightly enhanced values below the tropopause in comparison with the background profile. Within the framework of PV inversion various mechanisms are identified. Important contributions to the peak in N^2 are due to the pronounced cyclone–anticyclone asymmetry in the vertical structure of the tangential wind, and to the poleward advection of high values of PV from the subtropical lower stratosphere. Qualitatively, the key features of the composite profiles are in good agreement with observations above southern Germany that have recently been compiled.

1. Introduction

A recent observational study by Birner et al. (2002, hereafter BDS02) investigated the static stability in the extratropical tropopause region. The authors analyzed 10 yr (1990–99) of twice-daily radiosonde profiles from two stations in southern Germany (Munich and Stuttgart) with a vertical resolution of approximately 50 m. They produced a climatology by composing a large number of profiles with the themal tropopause as common reference level. The resulting buoyancy frequency squared N^2 is depicted schematically in Fig. 1 (solid line). The key features are a jump in N^2 right at the height z_{tp} of the thermal tropopause and a sharp maximum just above z_{tp}. Immediately beneath z_{tp} the values of N^2 are somewhat increased with respect to typical tropospheric values further below. While this result is likely to be representative for southern Germany, it remains for future studies to find out whether one obtains a similar picture throughout the midlatitudes.

These observations motivated us to investigate the thermal structure of the extratropical tropopause region from a more theoretical point of view. We ask the following question: what is the impact of conservative balanced dynamics on the profiles of static stability in the tropopause region? Our approach is similar to Wirth (2001, hereafter W01). Essentially, we specify axisymmetric distributions of potential vorticity (PV), perform PV inversion in order to obtain the related balanced wind and temperature fields (Hoskins et al. 1985), and analyze those fields paying special attention to the tropopause region. In particular we compute profiles of N^2 obtained for different anomalies and compose them in the same way as was done by BDS02, that is, with the thermal tropopause as common reference level. The anomalies are specified such that they can be interpreted as the result of a formation process implying adiabatic advection across the gradients of a smooth background atmosphere (cf. Fig. 2 later). Clearly this is an idealized approach that emphasizes fundamental properties of balanced flow. Rather than trying to be as realistic as possible we prefer to keep the setup simple in order to facilitate the interpretation. Nevertheless, the model turns out to qualitatively reproduce the essential features obtained by BDS02. This encourages us to carry through a detailed analysis yielding insight into the underlying mechanisms within the current framework.

In the analysis we shall consider ''related'' cyclones and anticyclones, which are treated identically except for the sign of their tropopause potential temperature anomaly $\Delta\theta$. It was shown in W01 that this leads—despite the (anti-) symmetry in $\Delta\theta$—to a pronounced *asymmetry* between cyclones and anticyclones regarding the height of the thermal and the dynamical tropopause. Not surprisingly, this cyclone–anticyclone asymmetry turns out to be relevant in our current problem, too.

Corresponding author address: Dr. Volkmar Wirth, Institute for Atmospheric Physics, University of Mainz, Becherweg 21, 55099 Mainz, Germany.
E-mail: vwirth@uni-mainz.de

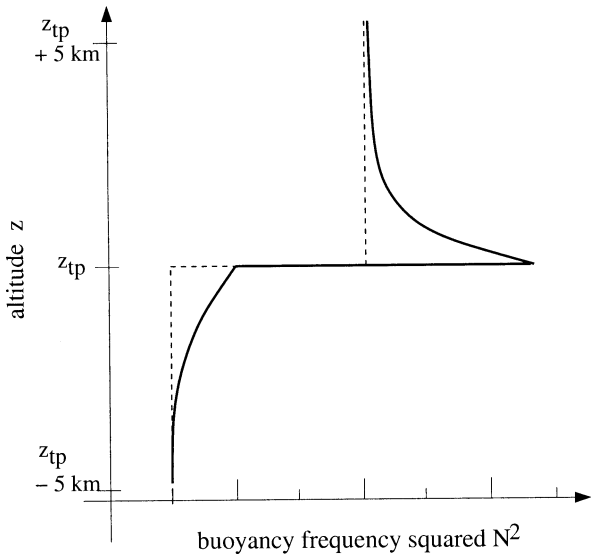

FIG. 1. Schematic representation of the climatological profile of N^2 in the tropopause region as observed by Birner et al. (2002) over southern Germany. The solid line corresponds to the high-resolution radiosonde data, and the dashed line depicts a hypothetical reference profile with piecewise constant N^2.

The paper is organized as follows. Section 2 briefly reviews the model and discusses how it is used in the present study. It is then applied in section 3 in order to successively unravel various mechanisms that contribute to shaping the thermal structure of the tropopause region. Finally, a summary and conclusions are provided in section 4.

2. Model

The model setup is essentially as in W01, which the reader may consult for the details. Here, only the main features will be presented as well as some modifications.

As an approximation to geometric altitude we use $z = -H\ln(p/p_0)$ as vertical coordinate, where p denotes pressure; $H = 7$ km is a constant mean scale height; and $p_0 = 1000$ hPa is a constant reference pressure. With this vertical coordinate the natural expression for the buoyancy frequency squared reads

$$N^2 = \frac{g}{T_s}\left(\frac{\partial T}{\partial z} + \frac{\kappa T}{H}\right), \tag{1}$$

where T is temperature, g denotes the acceleration due to gravity, $\kappa = R/c_p = 2/7$ is the ratio of the gas constant R and the specific heat c_p at constant pressure for dry air, and where T_s is defined through $RT_s = gH$ (see Andrews et al. 1987). We will refer to N^2 as static stability throughout this text. Potential vorticity is given by

$$Q = \frac{1}{\rho_0}\boldsymbol{\zeta}_a \cdot \boldsymbol{\nabla}\theta, \tag{2}$$

with density $\rho_0 = p/(RT_s)$, potential temperature $\theta = T\exp(\kappa z/H)$, and absolute vorticity $\boldsymbol{\zeta}_a$. On the level of approximation of the primitive equations the latter is given by $\boldsymbol{\zeta}_a = f\mathbf{k} + \boldsymbol{\nabla} \times \mathbf{v}$ with the horizontal wind $\mathbf{v}$ and the unit vector $\mathbf{k}$ in the vertical.

Figures 2, 3, and 4 illustrate the basic procedure. First, we specify a background atmosphere, which is characterized by smooth horizontal gradients in the troposphere and stratosphere and by a linear increase of the tropopause height with horizontal distance s (Fig. 2). The variable s is defined as the deviation of the tropopause potential temperature θ^{tp} from the constant value $\theta_0^{\text{tp}} = 330$ K. The background PV (gray shading in Fig. 2) is approximated as

$$\hat{Q}(s, z) = \frac{f_0}{\rho_0(z)}\frac{\partial\hat{\theta}}{\partial z}, \tag{3}$$

where $f_0 = 10^{-4}\ \text{s}^{-1}$ is the Coriolis parameter, and its profile at $s = 0$ will be called reference PV profile $Q_{\text{ref}}(z) = \hat{Q}(0, z)$. Since the background atmosphere is assumed to be shaped by processes that are not modeled explicitly, it implies some freedom, which we draw on by rendering the profile of N^2 as simple as possible. It is characterized by two constant values, one for the troposphere ($N_t^2 = 1 \times 10^{-4}\ \text{s}^{-2}$) and one for the stratosphere ($N_s^2 = 4 \times 10^{-4}\ \text{s}^{-2}$), and a smooth transition over a few hundred meters mediated by a hyperbolic tangent with a vertical scale of $\delta = 250$ m (Fig. 3). This profile, with the transition centered at the respective reference level, will be referred to as $N_{\text{ref}}^2(z)$ in the following. The (approximately) piecewise constant nature of $N_{\text{ref}}^2(z)$ makes it easy to focus on the changes brought about by the dynamics of the anomaly formation, which we intend to investigate in this study. Note that in W01 the lapse rate $\partial T/\partial z$ rather than N^2 was chosen to be the piecewise constant.

The construction of the f-plane PV anomaly from the background atmosphere is meant to emulate the formation of a cutoff cyclone or anticyclone implying a strongly nonlinear development from an initially zonal background flow (e.g., Palmén 1949). It is indicated in Fig. 2 through the arrows and explained in detail in W01. At the outer boundary of the computational domain we specify the PV profile to be equal to $Q_{\text{ref}}(z)$ and the profile of buoyancy frequency squared to be equal to $N_{\text{ref}}^2(z)$. In the interior we obtain an axisymmetric PV distribution

$$Q(r, \theta) = \frac{f_0 + \tilde{\zeta}}{\sigma}, \tag{4}$$

where r denotes radius,

$$\sigma = -\frac{1}{g}\frac{\partial p}{\partial\theta} = \frac{e^{-(\kappa+1)z/H}}{N^2}\frac{p_0}{HT_s} \tag{5}$$

is the density in isentropic coordinates, $\tilde{\zeta} = r^{-1}\partial(rv)/\partial r$ is the vertical component of relative vorticity in isentropic coordinates, and v is the tangential wind. The PV

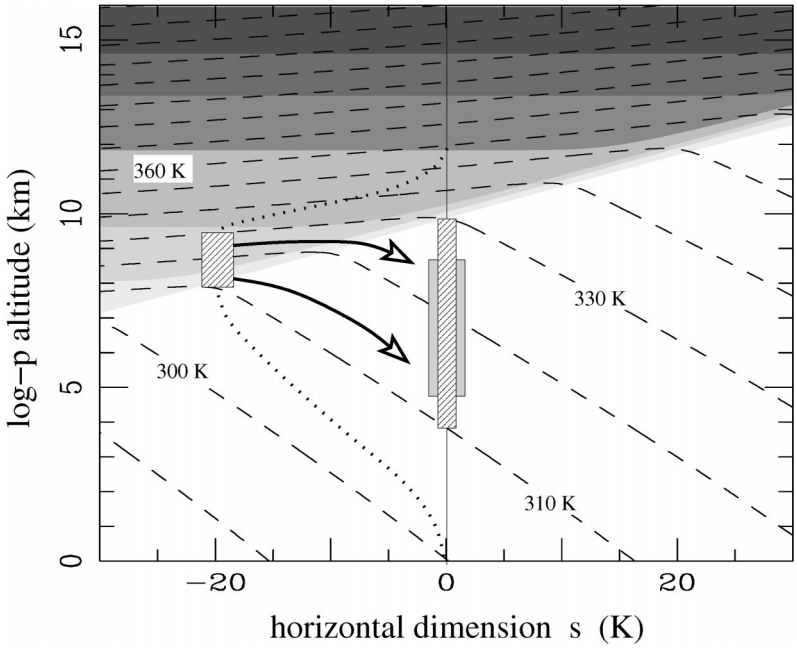

FIG. 2. Background atmosphere, which is used to construct the anomalies to be investigated. The dashed contours depict potential temperature θ (in K, contours every 10 K), and the shading indicates potential vorticity $\hat{Q}(s, z)$ (in PVU, where 1 PVU = 10^{-6} m^2 s^{-1} K kg^{-1} and where the steps in shading are at 2, 3, 4, 6, 8, and 10 PVU; light shading represents low values and dark shading high values of PV). The hatched vertical column at $s = -20$ K and the arrows illustrate the construction of a cyclonic anomaly invoking adiabatic advection. The thickness of the column at its final position (shaded column at $s = 0$ K) differs from its initial thickness owing to secondary vertical motions, which displace the isentropes during the formation of the anomaly.

anomaly is essentially characterized by two parameters, namely, the radial scale ΔR and the tropopause potential temperature anomaly $\Delta\theta$ in the center of the votex. Two examples are displayed in Figs. 4a,b. The dynamical tropopause is defined through $Q = 2.5$ PV units (PVU) and is delineated as the interface between the white and the dark shading in Fig. 4. The two anomalies in Figs. 4a,b differ by the sign of $\Delta\theta$, where the negative sign represents a cyclonic anomaly and the positive sign an anticyclonic anomaly. Such pairs of anomalies will be referred to as related cyclones and anticyclones in the following. Note that in this example the change in PV across the dynamical tropopause in the vortex center is less pronounced for cyclones than for anticyclones (see Figs. 4a,b). A modification to the background state, which we describe later in this paper, will investigate the impact of this particular feature on the results.

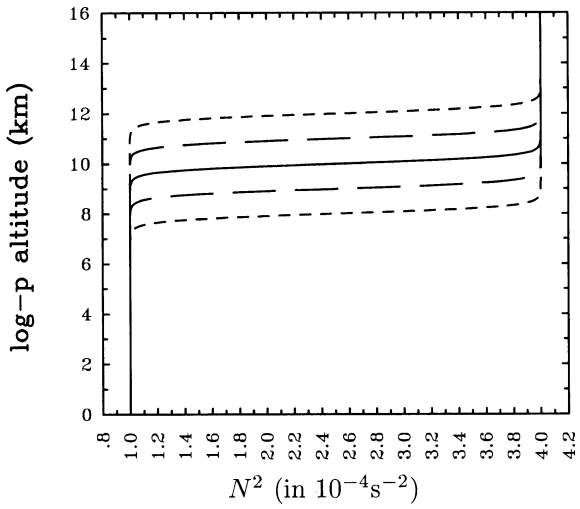

FIG. 3. Five profiles of static stability N^2 of the background atmosphere for five different values of the tropopause height.

Assuming hydrostatic and gradient wind balance the PV anomaly is ''inverted'' to obtain the wind and pressure field in isentropic coordinates. The boundary conditions are specified as described in W01. Unless noted otherwise, our results do not sensitively depend on that specification. Finally, transformation to z as vertical coordinate yields the axisymmetric f-plane vortices, which will be analyzed in the following. The result for our two sample vortices is displayed in Figs. 4c,d. The basic features in the tropopause region correspond well to those of the idealized vortices of Thorpe (1986), although in the latter work the PV anomaly is more localized. More importantly, they correspond well in the case of the cyclone to the features of observed cutoff cyclones (e.g., Fig. 10.8 in Palmén and Newton 1969;

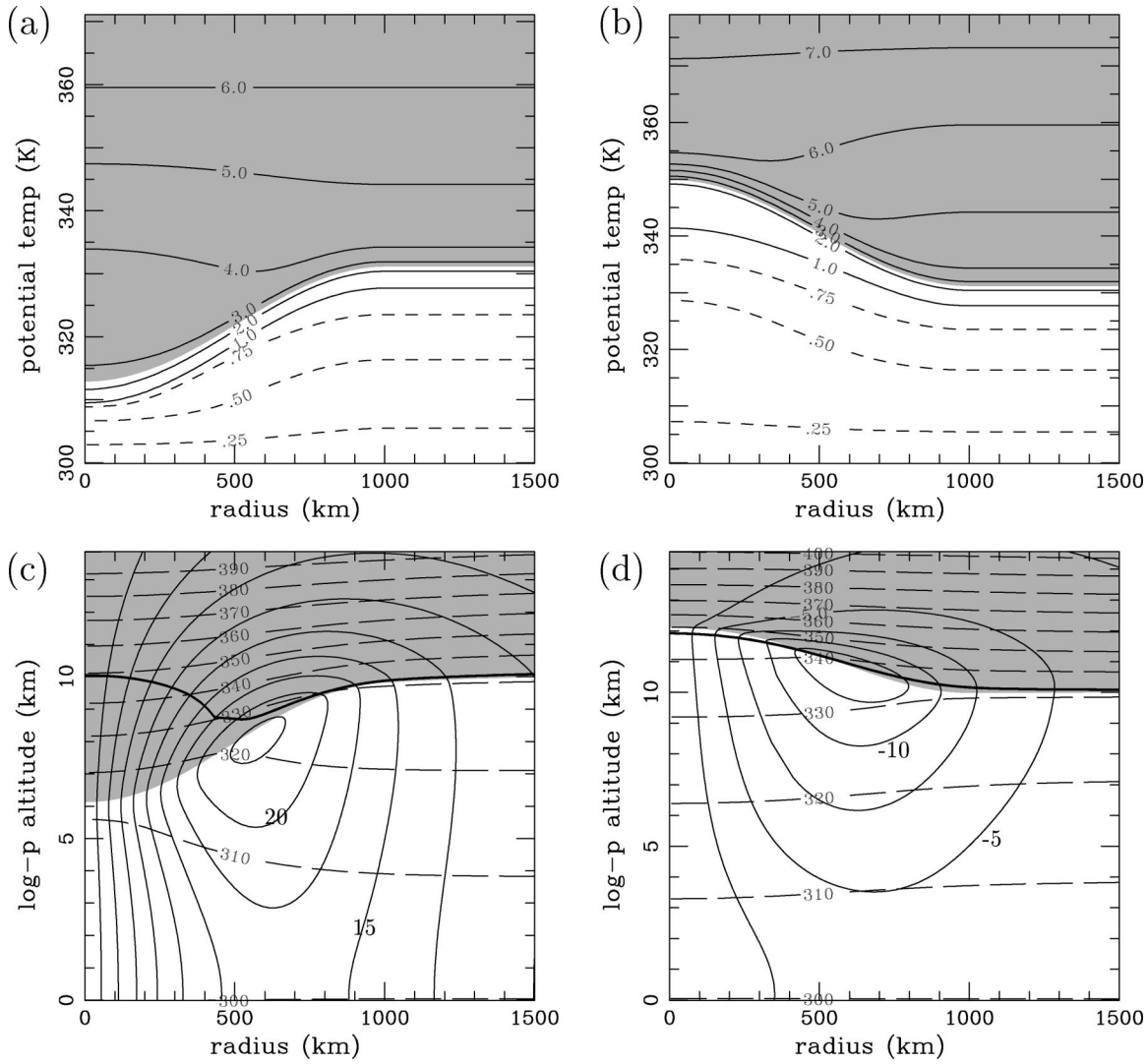

FIG. 4. Generation of axisymmetric anomalies on an f plane with $\Delta R = 1000$ km and $|\Delta\theta| = 20$ K for (a), (c) the cyclonic case and (b), (d) the anticyclonic case. (a), (b) The specified PV distribution $Q(r, \theta)$ in isentropic coordinates, and (c), (d) the vortices after PV inversion and transformation to z as vertical coordinate. (a)–(d) Gray shading indicates stratospheric values of PV, that is, $Q > 2.5$ PVU, and the dynamical tropopause is delineated by the interface between the white and the dark-shaded area. (a), (b) The contours are isolines of PV (in PVU). (c), (d) The solid contours depict tangential wind v (in m s^{-1}, contours every 2.5 m s^{-1}), while the dashed contours depict potential temperature (in K, contours every 10 K). The thick solid line in (c) and (d) is the thermal tropopause. Only part of the computational domain is displayed.

or Fig. 1.4.d in Newton and Holopainen (1990); and similar cross sections are obtained for upper-tropospheric shear lines (Appenzeller et al. 1996), which would correspond to plane symmetry rather than circular symmetry (cf. Wirth 2000). There is a noticeable asymmetry between the cyclonic and the anticyclonic vortex in Figs. 4c,d regarding the displacement of the dynamical tropopause in the vortex center and the strength of the tangential wind, which is reminiscent of the observed difference between strong upper-tropospheric cyclones and anticyclones (Muraki and Hakim 2001). Is was shown in W01 that this cyclone–anticyclone asymmetry has implications for the difference in altitude between the thermal tropopause (thick solid line in Figs. 4c,d) and the dynamical tropopause. As we shall see later, this difference between the two tropopauses plays a significant role for the composite profiles of N^2, too.

Vertical resolution is an important aspect in the current work. It is effectively determined by the smooth transition of N^2_{ref} between its tropospheric and its stratospheric value, which has a scale δ of a few hundred meters (see Fig. 3). The vertical grid spacing (about 70 m) is much smaller by comparison, which is desirable, as otherwise the results would strongly depend on the numerical resolution. The sensitivity with respect to δ will be addressed in section 4.

3. Results

The model is used in order to successively unravel the mechanisms that contribute to shaping the thermal structure in the tropopause region. The anomalies investigated in sections 3a through 3d have an amplitude of $\Delta\theta = \pm 20$ K. Since earlier studies have indicated the crucial role of the anomalies' aspect ratio (Wirth 2000), we consider two distinct values for the radial scale ΔR so as to investigate one case of a flat aspect ratio ($\Delta R = 2500$ km) and one case of an intermediate aspect ratio ($\Delta R = 500$ km). Very tall aspect ratios ($\Delta R \to 0$) are not considered explicitly, because the result is known a priori: in this limit the PV anomaly is realized entirely in terms of vorticity, and the thermal structure is determined by the outer boundary, which is specified from the reference atmosphere. As a consequence the profile of N^2 would be identical to the reference profile N^2_{ref}. Later, in section 3e we consider a whole range of values for ΔR and different values for $\Delta\theta$, and we retrieve profiles not only from the votex center but from different radii in order to test the robustness of the results.

a. Effect of PV advection

By construction, the reference profile $N^2_{\text{ref}}(z)$ is a piecewise constant with a smooth transition over a distance of a few hundred meters (see Fig. 3). However, in the center of the anomaly the tropopause region consists of air that has been advected quasi-horizontally some finite distance across the background atmosphere. This makes the PV profile at the vortex center deviate from the reference profile $Q_{\text{ref}}(z)$, because the background PV at the tropopause level varies with horizontal distance. To the degree that PV is materialized in terms of static stability, this modifies the profile of N^2 in comparison with N^2_{ref}.

We intoduce a new variable N^2_{stat} that quantifies the impact of the PV modification through advection. Assuming a static atmosphere, PV is given as

$$Q(z) = \frac{f_0}{\rho_0(z)}\frac{\partial\theta}{\partial z} = \frac{f_0 T_s}{g\rho_{00}} N^2(z) e^{(\kappa+1)z/H}. \tag{6}$$

Solving (6) for N^2 yields the ''static buoyancy frequency squared''

$$N^2_{\text{stat}}(z) = \frac{g\rho_{00}}{f_0 T_s} Q(z) e^{-(\kappa+1)z/H}, \tag{7}$$

which is the hypothetical profile of N^2 if a given profile of $Q(z)$ were realized in a static atmosphere. It expresses the PV profile in terms of a buoyancy frequency squared, which is the relevant quantity in the present context. The fact that the vortex center is, indeed, not part of a static atmosphere but rather embedded in a balanced flow will be considered further later.

The long dashes in Fig. 5 depict the profiles of $N^2_{\text{stat}}(z)$ at the vortex center for cyclonic and anticyclonic anomalies with $\Delta R = 2500$ km and $\Delta R = 500$ km, respectively. In each case there is a sharp increase of $N^2_{\text{stat}}(z)$ with altitude approximately at the location of the dynamical tropopause, which is located at $z = 5.9$, 12.6, 6.1, and 11.7 km in Figs. 5a–d, respectively. This is consistent with (7), because $N^2_{\text{stat}}(z)$ is proportional to $Q(z)$, and the latter features a sharp increase at the dynamical tropopause by construction. A quantitative comparison with $N^2_{\text{ref}}(z)$ indicates that generally $N^2_{\text{stat}}(z) > N^2_{\text{ref}}(z)$ for cyclonic conditions (left column in Fig. 5) and $N^2_{\text{stat}}(z) < N^2_{\text{ref}}(z)$ for anticyclonic conditions (right column in Fig. 5). Note that the profile $N^2_{\text{stat}}(z)$ is a result of the rearrangement of PV during the generation process, that is, horizontal advection on isentropes in combination with implied vertical displacement of the isentropes (cf. Figs. 2 and 4c for the cyclonic case). The net result depends on the balance between horizontal and vertical advection, which in turn depends on both the background PV and the details of anomaly construction. In the present case the implied lower-stratospheric downward displacement in the case of cyclones in combination with the positive vertical PV gradient in the background atmosphere is responsible for the increased values of N^2_{stat} above the tropopause. Similarly, the implied upward displacement in the case of anticyclones is responsible for the decreased values of N^2_{stat} above the tropopause.

None of the profiles of N^2_{stat} in Fig. 5 features a sharp peak right above the jump from tropospheric to stratospheric values. Therefore, it appears unlikely that the distinct features of the observed profiles of N^2 in Fig. 1 are related to the physical process encapsulated in N^2_{stat}.

b. PV partitioning

Our hypothetical quantity $N^2_{\text{stat}}(z)$ deviates from the actual static stability $N^2(z)$, because a given profile of PV materializes partly in terms of a thermal anomaly (static stability) and partly in terms of a dynamical anomaly (vorticity). A key parameter determining the partitioning between thermal and dynamical anomaly is the aspect ratio of the anomaly (cf. Wirth 2000).

The situation is analyzed in Fig. 5, where the solid lines denote the actual profile $N^2(z)$, and the short dashes denote

$$N^2_{\text{dyn}} = N^2(z) - N^2_{\text{sat}}(z), \tag{8}$$

that is, the difference between the actual and the hypothetical ''static'' profile. This difference will be called dynamical contribution in the following, as it is related to the presence of nonzero balanced flow. It implicitly includes the integrated effect of the secondary circulation during the process of the anomaly formation. Apparently, the dynamical contribution is negative for cyclones and positive for anticyclones. Equation (4) explains why: for a given value of Q, cyclonic flow with $\tilde{\zeta} > 0$ implies larger σ and, according to (5), smaller

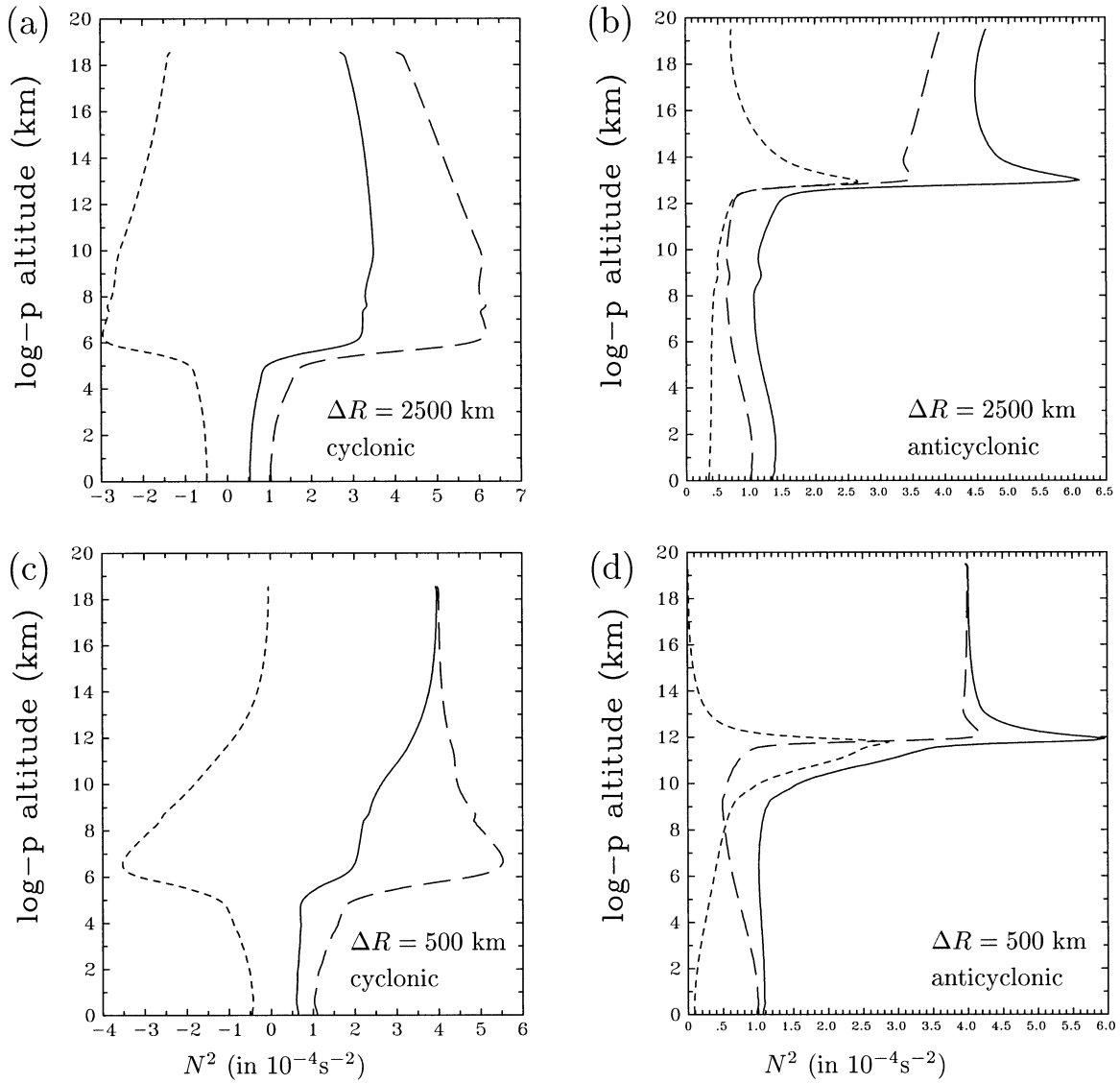

FIG. 5. Profiles of static stability N^2 in the vortex center, for (a) a cyclonic anomaly with $\Delta R = 2500$ km, (b) an anticyclonic anomaly with $\Delta R = 2500$ km, (c) a cyclonic anomaly with $\Delta R = 500$ km, and (d) an anticyclonlic anomaly with $\Delta R = 500$ km. The amplitude is fixed at $|\Delta\theta| = 20$ K in all four cases. (a)–(d) The solid line denotes the actual profile $N^2(z)$, the long dashes denote the hypothetical ''static'' profile $N^2_{\text{stat}}(z)$, and the short dashes denote the ''dynamical contribution'' $N^2_{\text{dyn}}(z) = N^2(z) - N^2_{\text{stat}}(z)$.

N^2 than a hypothetical static situation with $\tilde{\zeta} = 0$; the opposite is true for anticyclonic flow. In all four cases N^2_{dyn} has its extreme value close to the dynamical tropopause. More importantly, N^2_{dyn} overcompensates the effect of the PV advection: in contrast with N^2_{stat} the actual profile N^2 (solid line) generally shows smaller values than N^2_{ref} in the case of cyclones and larger values than N^2_{ref} in the case of anticyclones. In this sense the dynamical contribution must be considered as the dominating mechanism. The net result is a destabilization in the tropopause region for cyclonic anomalies and a stabilization for anticyclonic anomalies. This general feature has been discussed before by several authors (Hoskins et al. 1985; Thorpe 1985, 1986; Bishop and Thorpe 1994; Thorpe and Bishop 1995) and is illustrated in our Figs. 4c,d as the anomalous spacing between the isentropes in the center of the anomaly.

There are systematic differences between the four cases in Fig. 5 regarding N^2_{dyn}. It is significantly more peaked for anticyclonic vortices (right column) than for cyclonic vortices (left column). In addition, the stratospheric penetration is smaller for taller anomalies (lower row) than for the corresponding flat anomalies (upper row). For an explanation we point out, again, that the dynamical contribution N^2_{dyn} is related to the vorticity of the balanced flow, that is, the tangential wind of the vortex. The difference in the vertical structure for the different values of ΔR is consistent with the concept of

''Rossby height'' (Hoskins et al. 1985), which relates the vertical penetration to the horizontal extension in the case of a localized PV anomaly. The difference between cyclones and anticyclones can be traced back partly to the nonlinearity of the PV inversion [Eqs. (6) and (7) in W01] and partly to the transformation from θ to z as vertical coordinate, which both contribute in the same sense to enhance the sharpness of the peak in the case of anticyclones, but lessen it in the case of cyclones. As noted before, PV inversion is performed iteratively. The solution from the first step in the iteration, which corresponds to the quasigeostrophic approximation (see Hoskins et al. 1985), shows only a minor cyclone–anticyclone asymmetry regarding the shape of the wind field $v(r, \theta)$, but as the iteration proceeds the solution becomes more peaked for anticyclones and less peaked for cyclones. This asymmetry is further enhanced through the vertical coordinate transformation owing to the fact that the spacing between isentropes above and below the tropopause is smaller in comparison with the reference atmosphere for anticyclones, but larger for cyclones (cf. Figs. 4d and 4c).

By definition of N^2_{stat} and N^2_{dyn} we have

$$f_0 N^2_{\text{stat}} = (f_0 + \tilde{\zeta})N^2 = (f_0 + \tilde{\zeta})(N^2_{\text{stat}} + N^2_{\text{dyn}}), \quad (9)$$

which can be rewritten as

$$N^2_{\text{dyn}} = F N^2_{\text{stat}} \quad \text{or} \quad (10)$$

$$N^2 = (F + 1)N^2_{\text{stat}} \quad (11)$$

where the dimensionless factor F is given by

$$F = -\frac{\tilde{\zeta}}{f_0 + \tilde{\zeta}}. \quad (12)$$

This formulation reveals how the ratio between N^2_{dyn} or N^2 and N^2_{stat} depends on the isentropic vorticity $\tilde{\zeta}$ and, hence, on the tangential wind v. Figure 6 shows F as a function of z in the vortex center for the four cases corresponding to Figs. 5a–d. The features pointed out before regarding N^2_{dyn} are reflected in corresponding features of F. Since our balanced vortices satisfy $\tilde{\zeta} > -f_0$ everywhere, the factor F is negative for cyclonic flow and positive for anticyclonic flow. The extremum of F is close to the dynamical tropopause (although small deviations turn out to be important). The stratospheric penetration is smaller for taller anomalies ($\Delta R = 500$ km) than for shallow anomalies ($\Delta R = 2500$ km), and F is significantly more peaked for anticyclones than for the corresponding cyclones. The latter feature is rendered plausible by examining the behavior of F in the limit of very strong cyclones ($\tilde{\zeta} \to \infty$) and anticyclones ($\tilde{\zeta} \to -f_0$), respectively. In the cyclonic case one obtains $F \to -1$, whereas in the anticyclonic case one obtains $F \to +\infty$. In other words, the asymmetry in the sharpness of the peak of N^2_{dyn} reflects the asymmetry between strong cyclones and anticyclones regarding their relative vorticity.

Adding the dynamical contribution N^2_{dyn} to the hypothetical profile N^2_{stat} yields the actual profile $N^2(z)$ depicted by the solid line in Fig. 5. For the anticyclonic vortices (Figs. 5b,d) the peak of N^2 just above the dynamical tropopause is much more pronounced than that of $N^2_{\text{stat}}(z)$, while for the cyclonic vortices $N^2(z)$ is either close to the reference profile (Fig. 5a) or features a more gradual transition from low-tropospheric values to high-stratospheric values (Fig. 5c). Clearly, the dynamical contribution substantially helps to produce a sharp peak in the profile of $N^2(z)$ for anticyclonic vortices. Note also that in Fig. 5d the dynamical contribution N^2_{dyn} gives rise to enhanced values of N^2 in a layer of a few kilometers below the peak.

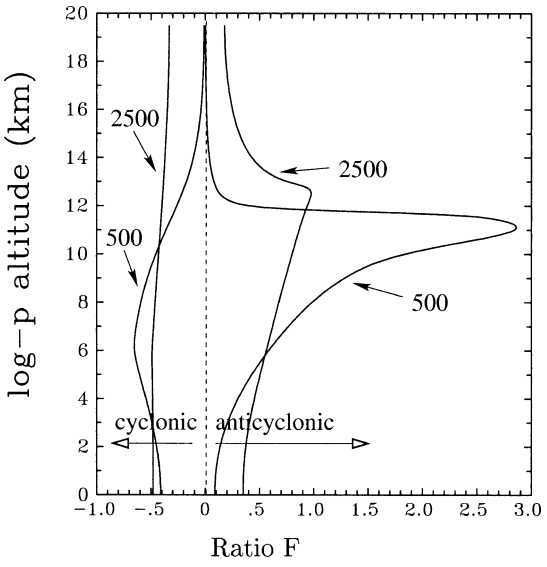

FIG. 6. Ratio $F = N^2_{\text{dyn}}/N^2_{\text{stat}}$ as a function of z in the vortex center. The four solid lines correspond to Figs. 5a–d; they are labeled according to the radial scale ΔR (km) of the vortex. The dashed line is the zero line, negative values of F are associated with cyclonic vortices, and positive F are associated with anticyclonic vortices.

As a next step we average related cyclonic and anticyclonic profiles from the vortex center using the dynamical tropopause as a common reference level. The dynamical tropopause as the reference level appears most natural, since this is approximately the location where Q, N^2_{stat}, and N^2 have their sharpest increase with altitude. Figures 7a and 7b show the results for $\Delta R = 2500$ km and $\Delta R = 500$ km, respectively. Both panels depict the average (solid line) of the cyclonic (long dashes) and the anticyclonic (long–short dashes) profiles. For comparison, the short dashes depict the reference profile N^2_{ref}. For both values of ΔR the average profile is characterized by a distinct peak just above the reference level. For $\Delta R = 500$ km one obtains increased values of N^2 (with respect to N^2_{ref}) in a layer of a few kilometers below the reference tropopause, which is associated with the behavior of N^2_{dyn}. The fact that averaging cyclonic and anticyclonic profiles leaves one with a nontrivial deviation from the reference profile is, to some degree at least, related to the asymmetry in the dynamical con-

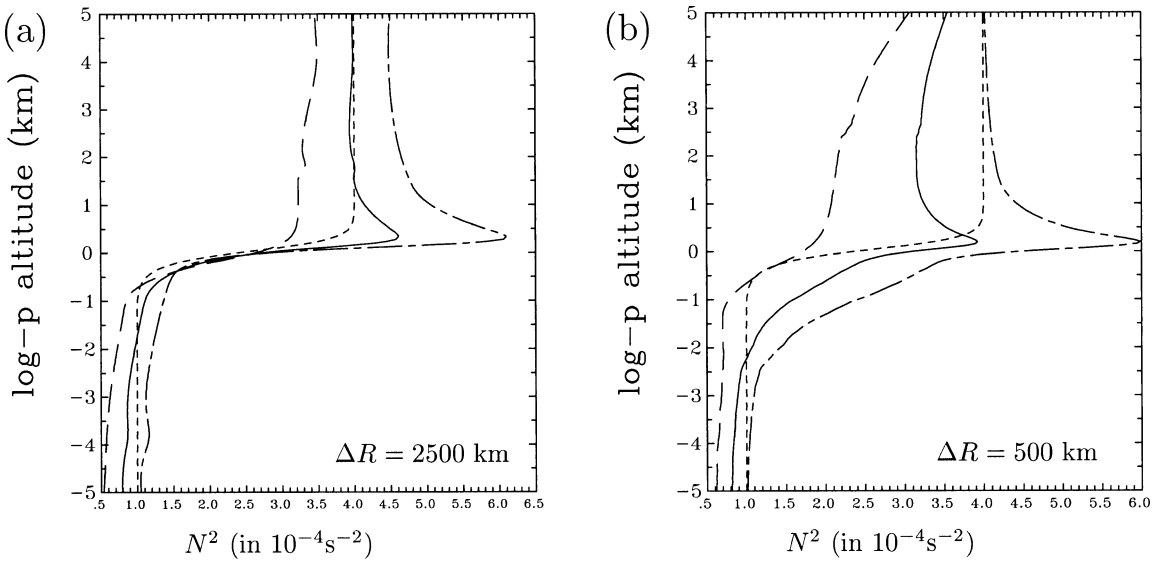

FIG. 7. Profiles of static stability N^2 in the vortex center, displayed such that the dynamical tropopause (at $z = 0$) is used as the common reference level, for (a) $\Delta R = 2500$ km and (b) $\Delta R = 500$ km. The vertical axis is relative distance with respect to the reference level. The lines with the long and long–short dashes depict the profiles for the cyclonic and anticyclonic vortex, respectively; the solid line is the average. The short dashes show the reference profile $N^2_{\text{ref}}(z)$ for comparison.

tribution between cyclones and anticyclones discussed earlier.

BDS02 used the thermal tropopause rather than the dynamical tropopause as the common reference level, because the former is much easier to diagnose from the observations. This is the source for another important asymmetry between cyclones and anticyclones, which was discussed in detail in W01. While the two tropopauses generally are rather close together for anticyclones, one expects substantial deviations for cyclonic anomalies of intermediate aspect ratio (cf. Figs. 4c and 4d), such that on average the thermal tropopause is located above the dynamical tropopause. If one chooses to define the reference level through the thermal tropopause, one thus obtains on average increased values of N^2 below the reference level. Figure 8 shows the composite profiles in the same format as in the previous figure, except that now the thermal tropopause is used as the common reference level. As before, the average profiles for both values of ΔR are characterized by a distinct peak above the reference level, but now the increase of N^2 (with respect to N^2_{ref}) below the reference

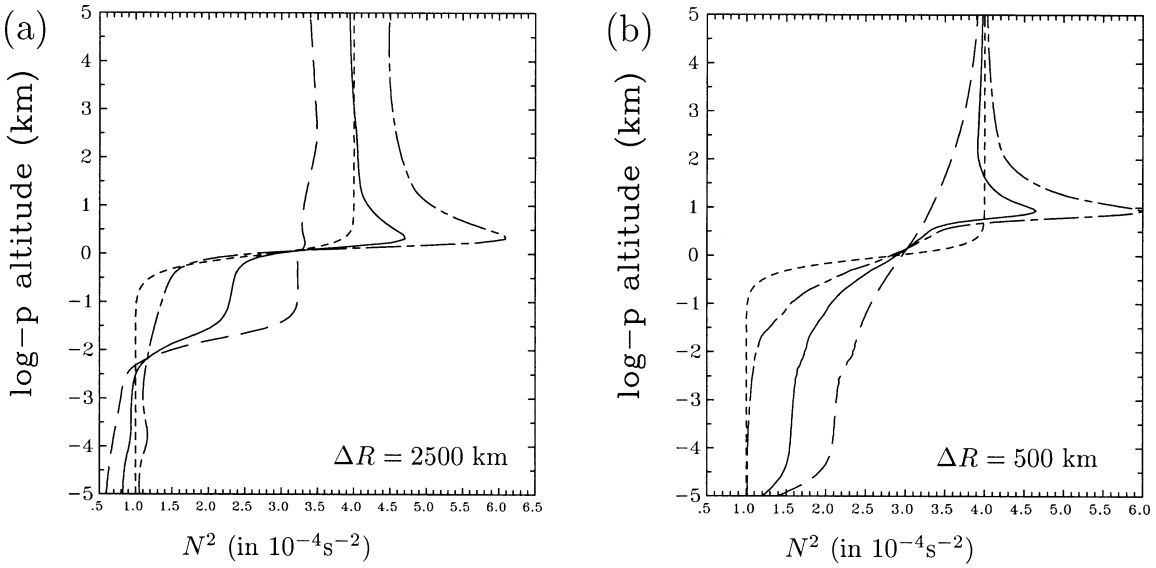

FIG. 8. Same as in Fig. 7 but with the thermal tropopause as the common reference level.

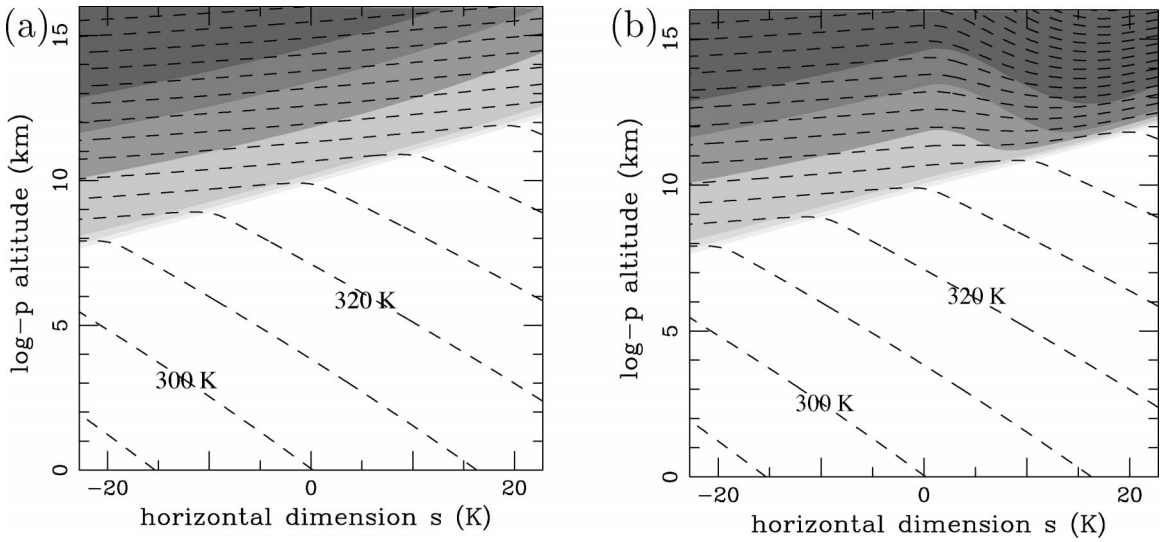

FIG. 9. Background atmosphere for two sensitivity experiments, (a) including the β effect, and (b) including both the β effect and increased stratospheric N^2 in the subtropics. The dashed lines denote potential temperature θ and the shading denotes PV as in Fig. 2.

level is more pronounced, and in the case of $\Delta R = 500$ km the peak is displaced slightly upward. Both features are associated with the displacement between the thermal and the dynamical tropopause and can, in this sense, be considered as artifacts. Nevertheless, even with the thermal tropopause as reference level the strong peak from the anticyclonic dynamical contribution survives the averaging procedure. Unless stated otherwise we will use the thermal tropopause as the reference level from now on.

We conclude that in our model the dynamical contribution relating a static PV profile to the actual static stability in a dynamical vortex is a key ingredient for shaping the thermal structure of the tropopause region.

c. β effect

So far we considered a background atmosphere with no horizontal variation of PV except across the tropopause (Fig. 2). However, if the background state were to represent a zonal mean atmosphere with latitude as horizontal coordinate, it would be more consistent to include an overall increase of PV with increasing latitude in the spirit of the β effect. We simulate this through replacing f_0 in (3) by $f(s) = f_0(1 - Bs)$ with $B = (60\ \mathrm{K})^{-1}$. The modified background atmosphere is shown in Fig. 9a. Note that the modification leaves both the reference temperature and $N^2_{\mathrm{ref}}(z)$ unchanged, but it changes the PV distribution leading to a nonzero horizontal gradient in both the troposphere and the stratosphere. With the chosen value of B the isolines of PV in the tropopause region are approximately parallel to the tropopause. As a consequence, given a thin layer above the tropopause, PV hardly varies with horizontal distance in that layer. This behavior contrasts with the situation considered so far (and depicted in Fig. 2), where the PV values in the lowest part of the stratosphere are lower in ''polar latitudes'' (with a low tropopause) than in ''subtropical latitudes'' (with a high tropopause).

The resulting composite profiles are displayed in Fig. 10 and should be compared with those in Fig. 8. The two cases (β and no-β) are broadly similar, but some differences are noteworthy. First, consider $\Delta R = 2500$ km. Including the β effect, even the cyclonic anomaly (long dashes in Fig. 10a) features a broad maximum of $N^2(z)$ above the tropopause, while for the anticyclonic anomalies (long–short dashes) the maximum is less pronounced than without β. The analysis (no figure shown) reveals that the cyclonic maximum is a feature of the static profile $N^2_{\mathrm{stat}}(z)$. The modified background atmosphere combined with our method of anomaly construction implies a layer of approximately constant PV above the tropopause in the cyclonic anomaly. Owing to the decaying exponential in (7) this leads to a decrease of N^2_{stat} with a vertical-scale height $H/(\kappa + 1) = 7H/9$ yielding a relative maximum in N^2_{stat} just above the tropopause. This relative maximum is only partly compensated by the dynamical contribution, because the latter is not very localized in the cyclonic case (similar to before; see Fig. 5). Note also that our β effect renders the displacement between thermal and dynamical tropopause in the cyclonic case less pronounced than previously. As a consequence, there is less of a ''misplacement'' of the reference level, which explains why in Fig. 10a one observes purely tropospheric values of N^2 up to the reference level, in contrast to the situation in Fig. 8a.

For anticyclonic flow the β effect works in the opposite direction: the static profile $N^2_{\mathrm{stat}}(z)$ (not shown) features a significantly smoother transition from tropospheric to stratospheric values such that the dynam-

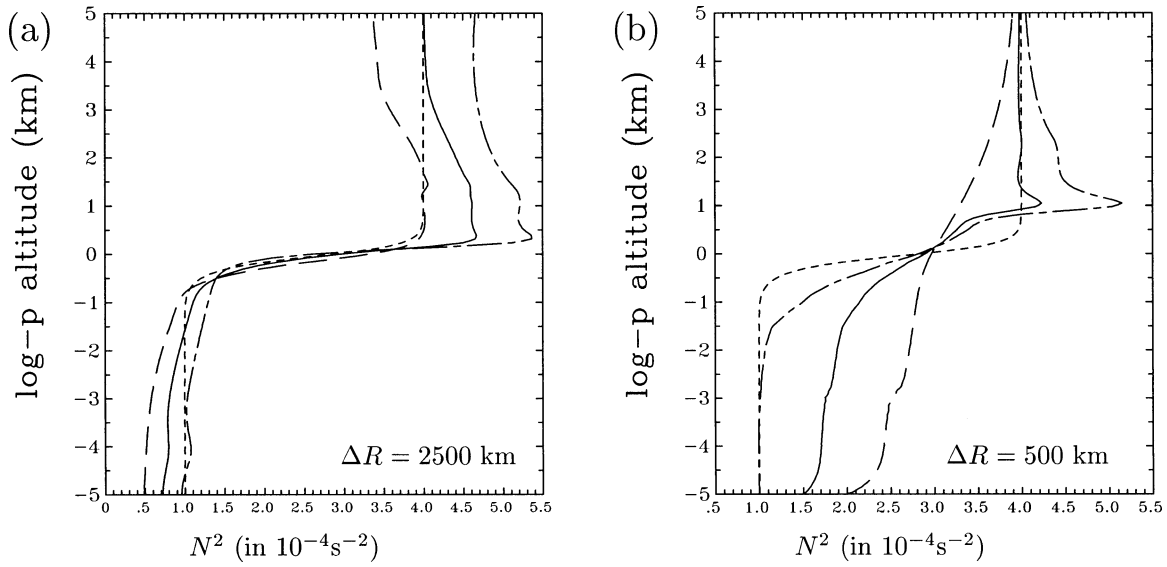

FIG. 10. Same as in Fig. 8 but for the experiment including the β effect in the background atmosphere (see Fig. 9a).

ical contribution (being very similar as before) is just able to produce a weak (yet noticeable) peak in Figs. 10a,b (long–short dashes, to be compared with the same lines in Fig. 8). We conclude that our β effect primarily modifies $N^2_{\text{stat}}(z)$ through changes in advected PV. The difference in behavior between cyclones and anticyclones is less pronounced than before.

d. Subtropical tropopause region

In the real atmosphere, temperature profiles in low latitudes are characterized by a sharp increase from a negative to a positive vertical gradient across the tropopause (e.g., Defant and Taba 1957), while in middle and high latitudes the lower stratosphere tends to be approximately isothermal. In other words, the lower-stratospheric static stability is higher in low latitudes than in high latitudes. This feature presumably results from processes (such as radiation) that operate on timescales longer than the dynamical timescales considered here. In the context of the present model it should be accounted for as a property of the background atmosphere. It is implemented through a modification of the background atmosphere ''south'' of the reference latitude (i.e., modifying those profiles for which the tropopause is higher than 10 km) by multiplying N_s^2 with a factor which is an increasing function of s. The result is shown in Fig. 9b. For $s = 20$ K the lower-stratospheric temperature gradient is roughly equal to $+10$ K km^{-1}, which is at the upper end of the observed range. At first glance the subtropical distributions of PV and θ in Fig. 9b may appear somewhat unrealistic. Note, however, that s is proportional to latitude only as long as the zonal mean tropopause temperature increases linearly with latitude, which is not the case in the neighborhood of the subtropical jet. We believe that our simple modification is meaningful in the current framework, as it focuses on the essential aspect, which is the advection of high values of stratospheric PV during the formation of anticyclones. Note that the β effect is included in this experiment as well.

By construction, cyclonic vortices are not affected by this modification; but for anticyclonic vortices the hypothetical profile N^2_{stat} (not shown) acquires a more pronounced maximum right above the tropopause, which is further enhanced through the dynamical contribution N^2_{dyn}. The combined effect is shown in Fig. 11, where for both values of ΔR the sharp peak from the anticyclonic vortex (long–short dashes) is strong enough to yield a pronounced peak even after averaging with the related cyclonic profile. Broadly speaking, the increased static stability in the lowest part of the subtropical stratosphere overcompensates the smoothing resulting from the β-effect in the case of anticyclonic vortices.

e. Average effect

So far we restricted our analysis to profiles taken from the center of four different vortices, which were characterized by two different values of ΔR and $\Delta\theta$, each. It is not straightforward to compare these profiles with the observed composite sketched in Fig. 1, since a stationary observer encounters a wide spectrum of vortices of different sizes and amplitudes. In addition, it is highly unlikely that all the measurements are done at the very time when the vortex center is overhead. In this study we are not trying to simulate realistic station statistics corresponding to Fig. 1, because this would require a statistical analysis regarding the size and strength of upper-tropospheric vortices above southern Germany, which is beyond the scope of this paper. In particular, we do not make any assumption about the asymmetry

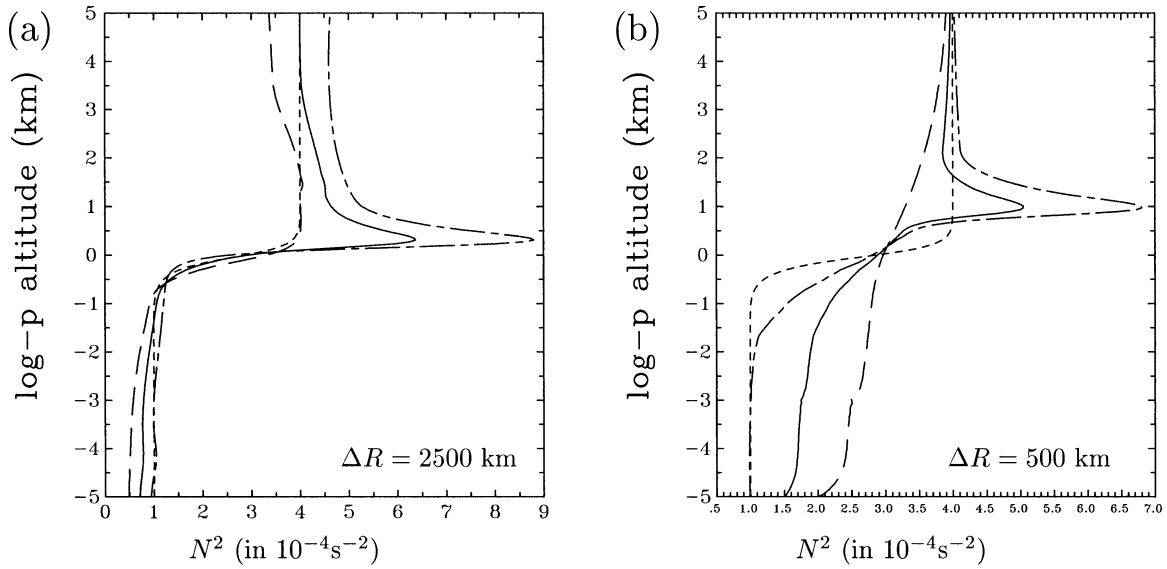

FIG. 11. Same as in Fig. 8, but for the experiment including the β effect in the background atmosphere as well as increased static stability in the subtropical lower stratosphere (see Fig. 9b).

between cyclones and anticyclones regarding their distribution in terms of amplitude $|\Delta\theta|$, but rather continue to compose related cyclones and anticyclones differing only by the sign of $\Delta\theta$.

Nevertheless we want to assure the robustness of our results by investigating whether (or to what extent) they remain valid when key parameters are changed. First, we vary ΔR over the range 500–2500 km with $|\Delta\theta| = 20$ K kept fixed. More specifically we use $\Delta R = 500$ km $+ (k - 1) \times 250$ km ($k = 1, 2, \ldots, 9$). The lower part of this range is meant to cover strongly nonlinear coherent structures in the tropopause region. A 33-yr climatology of such structures in the extratropics compiled by Hakim (2000) revealed typical radial scales of 500–800 km, which translates to $\Delta R = 750$–1200 km in our notation, while the study of Zängl and Wirth (2002), which focuses on higher latitudes, suggests smaller values ($\Delta R \approx 500$ km). The high end of our range for ΔR is meant to account for the effect of large-amplitude synoptic-scale waves. Both the β effect and the increased static stability in the subtropical stratosphere are included as described above, and again only profiles from the vortex center are used. Averaging the 2×9 profiles thus obtained one arrives at the composite shown in Fig. 12a (solid line). Apparently, the essential features pointed out before are also present in this average, most notably the peak in N^2 above the tropopause. The analysis reveals that it is mostly the anticyclonic profiles contributing to this peak, while the cyclonic profiles weaken and slightly smooth the step of N^2 across the tropopause. However, the anticyclonic profiles dominate the average.

The analysis is repeated with the dynamical tropopause as the common reference level, since (as pointed out before) this would be a more natural choice. The result is shown in Fig. 12b. Indeed, the peak is somewhat narrower than before and the values of N^2 are less enhanced below the reference level.

The composite from Fig. 12a cannot be compared yet with the observed composite sketched in Fig. 1, because all the profiles inherent in the average of Fig. 12 are taken from the centers of various different vortices. When each of these vortices is used to extract six different profiles at six different radii $r_k = (k - 1)\Delta R/6$ ($k = 1, 2, \ldots, 6$), we obtain the composite shown in Fig. 13a (solid line). The peak above the tropopause as well as the enhanced values below the tropopause (with respect to N^2_{ref}) are still noticeable, although both features are less pronounced than in Fig. 12a. Qualitatively, the mean profile in Fig. 13a agrees well with the observed behavior sketched in Fig. 1. The experiment was repeated with $|\Delta\theta| = 10$ K instead of $|\Delta\theta| = 20$ K. The resulting profile is qualitatively very similar to that shown in Fig. 13a, but the amplitude of the peak is reduced by roughly 50%.

It is also interesting to compute average profiles of tangential wind v with the same composing technique as for N^2, that is, using the thermal tropopause as common reference level. The result is shown in Fig. 13b (solid line). In contrast to $N^2(z)$, the wind in the tropopause region sensitively depends on the upper and lower boundary conditions for v when performing PV inversion. If we use zero Dirichlet instead of our standard treatment (which is zero Neuman), we obtain the dashed profile in Fig. 13b. Despite the strong sensitivity with respect to the boundary conditions, the qualitative features are very similar in both profiles, with a peak slightly below the tropopause and a stronger decay above the tropopause than below. Both features are pres-

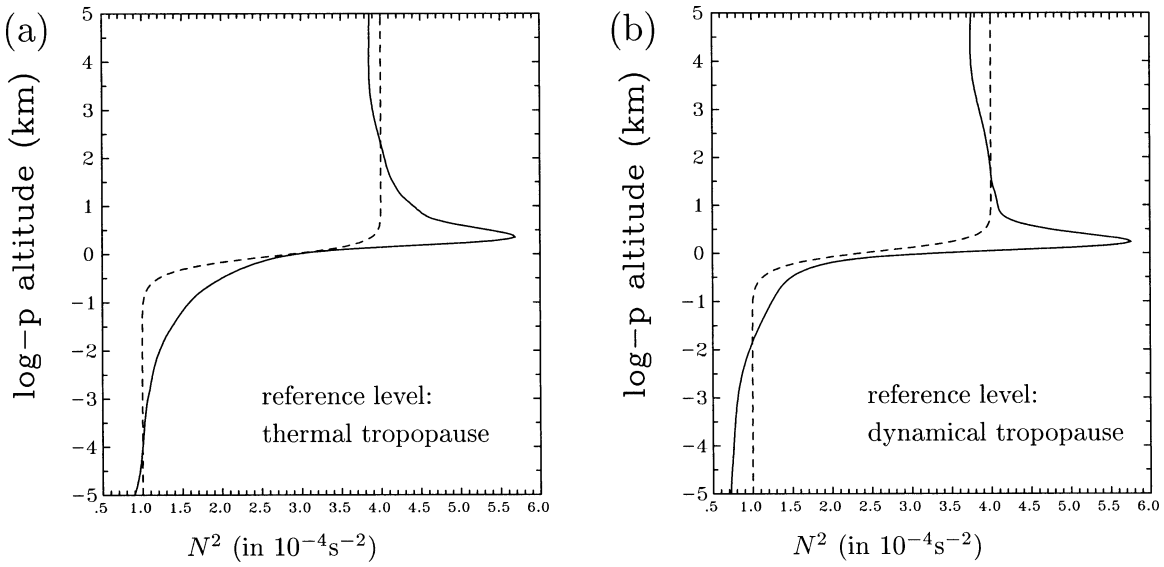

FIG. 12. Composite profiles of static stability N^2 in the vortex center, displayed such that (a) the thermal tropopause and (b) the dynamical tropopause is used as the common reference level (located at $z = 0$). The composite (solid line) is an average over several vortices with different radial scale ΔR, but with the amplitude fixed at $|\Delta\theta| = 20$ K. The short dashes show the reference profile $N^2_{\text{ref}}(z)$ for comparison. The vertical axis is relative distance with respect to the reference level.

ent in the observations of BDS02 (see their Fig. 2a), which strengthens our case.

4. Summary and conclusions

This study is motivated by the observations of BDS02, who showed that the buoyancy frequency squared N^2 in the extratropical tropopause region has a characteristic profile with a sharp peak just above the tropopause and slightly enhanced values below the tropopause in comparison with typical tropospheric values further below. A major aspect of that study is the method of composing different profiles, which implies an averaging procedure with the thermal tropopause used as

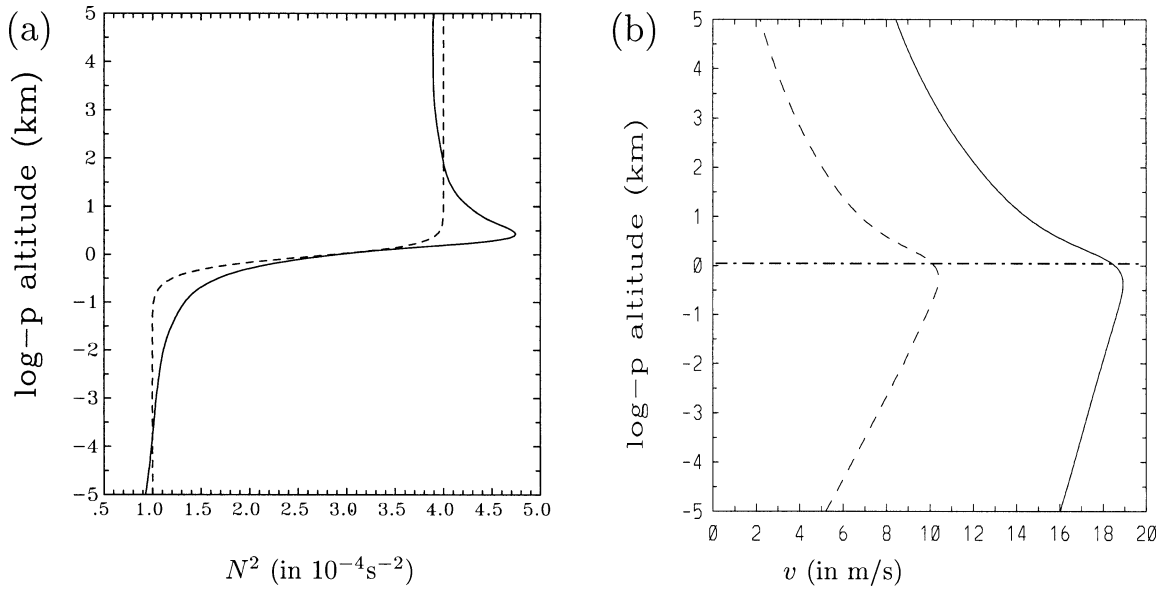

FIG. 13. Composite profiles of (a) buouancy frequency squared N^2 and (b) tangential wind v, for vortices with amplitude $|\Delta\theta| = 20$ K. The average was taken over $2 \times 9 \times 6$ different profiles involving nine cyclonic vortices of different radial scale ΔR, their related anticyclones, and using each of these 18 vortices to extract profiles at six different radii r_k ($k = 1, 2, \ldots, 6$). (a) The solid line depicts $N^2(z)$, while the dashed line depicts the reference profile $N^2_{\text{ref}}(z)$. (b) The solid line corresponds to the standard (zero Neuman) lower and upper boundary conditions, while the dashed line represents zero Dirichlet lower and upper boundary conditions. The dash–dotted line in (b) indicates the location of the thermal tropopause.

common reference level. Here we ask the following question: given a background atmosphere with a well-defined tropopause, what is the impact of conservative balanced dynamics on the profiles of static stability in the tropopause region, and may the observed composite be at least partly due to balanced dynamics? In our analysis we assume a background atmosphere that is characterized by a sloping tropopause and a simple reference profile N^2_{ref} for the static stability. Axisymmetric balanced flow anomalies are constructed implying conservative PV advection across the gradients of this background atmosphere. Effectively the method reduces to the specification of PV anomalies in isentropic coordinates, PV inversion, and subsequent transformation to altitude as vertical coordinate. Related cyclones and anticyclones differ only by the sign of the tropopause potential temperature anomaly $\Delta\theta$. The analysis focuses on the profiles of $N^2(z)$ as a function of altitude in the tropopause region. When composing profiles from different vortices including both cyclones and anticyclones, we follow BDS02 using the thermal tropopause as the common the reference level. The profiles of N^2 thus obtained show characteristic deviations from the reference profile N^2_{ref}, which in the present model are by necessity due to the impact of balanced dynamics. These deviations tend to be positive in a shallow layer above the tropopause, suggesting that balanced dynamics, indeed, contribute to the observed peak.

In the analysis it proves helpful to distinguish two mechanisms. First, specific properties of the background atmosphere have an impact, since they are advected during the anomaly formation. This mechanism materializes in the form of a local PV anomaly and is quantified through a hypothetical profile N^2_{stat}, which is defined as the static stability of given PV profile if the latter were realized entirely in terms of static stability. Second, there is a dynamical contribution N^2_{dyn} arising from the fact that a given PV distribution is not entirely materialized in terms of static stability, but to a certain degree in terms of vorticity, thus leading to a modification in comparison with the hypothetical static situation. In mathematical terms this dynamical contribution reflects the solution of the elliptic PV inversion equation.

Using the preceding terminology we summarize our analysis as follows.

- A major systematic impact in our model arises from the dynamical contribution N^2_{dyn}. The latter is positive and has a sharp peak right around the dynamical tropopause for anticyclones; it is negative and much less peaked in the case of cyclones. Owing to this asymmetry the anticyclonic peak dominates the composite.
- The ratio F between N^2_{dyn} and N^2_{stat} can be expressed in terms of isentropic relative vorticity $\tilde{\zeta}$ as $F = N^2_{\text{dyn}}/N^2_{\text{stat}} = -\tilde{\zeta}/(f_0 + \tilde{\zeta})$, where f_0 is the Coriolis parameter. It follows that the asymmetry in N^2_{dyn} between cyclones and anticyclones is related to the asymmetry in $\tilde{\zeta}$, which is bounded below by $-f_0$ for anticyclonic balanced flow, but which has no upper bound for cyclonic balanced flow.
- The advection of PV across the background atmosphere may have a significant impact on the profile of N^2_{stat}, but the related modification generally depends on the details of the background atmosphere as well as the anomaly formation. We identified two aspects of the background atmosphere (next two list items) that are likely to contribute in a systematic way to the profile of N^2 through the advective mechanism.
- The β effect, that is, the fact that the absolute value of planetary vorcitity is larger in regions where the tropopause is lower, leads to slightly increased values of N^2 just above the reference level in the case of strong cyclones, but it is unlikely to produce a very sharp peak in a climatological composite.
- Advection of high static stability from the subtropical lower stratosphere may significantly contribute to the peak of N^2 above the reference level in the case of anticyclones.
- Enhanced values of N^2 below the reference level may be due to both cyclones and anticyclones of intermediate aspect ratio. As is known from previous work, there may be a displacement between the dynamical and the thermal tropopause. This displacement is largest in the case of cyclonic anomalies of intermediate aspect ratio, for which the thermal tropopause is located significantly above the dynamical tropopause (cf. Fig. 4c). In the present context, where the reference level is defined through the thermal tropopause, this yields increased values of N^2 in the upper troposphere. Likewise one obtains enhanced values of N^2 for anticyclones of intermediate aspect ratio, since in that case N^2_{dyn} is positive and extends a few kilometers below the peak (Fig. 5d).
- We computed average profiles drawn from different radii r_k and using vortices with different radial scale ΔR. The resulting composite profiles of N^2 agrees very well with the observed profile in a qualitative sense, although the peak is less pronounced in our model. Repeting this analysis for the tangential wind v we obtained, again, good qualitative agreemend regarding the key features observed by BDS02.
- The dynamical tropopause would be a more natural choice as the reference level than the thermal tropopause, because the former is related to a strong increase in PV with altitude, which is reflected in similar behaviour of N^2. As a consequence, the peak in N^2 above the reference level would be more pronounced for the composite profile when the reference level is defined through the dynamical tropopause.

With the present numerical technique it is difficult to properly treat very large gradients and near discontinuities. This is the rationale behind the smooth transition between tropospheric and stratospheric values of N^2 in the background atmosphere (cf. Fig. 3), and it may be part of the reason why in our model

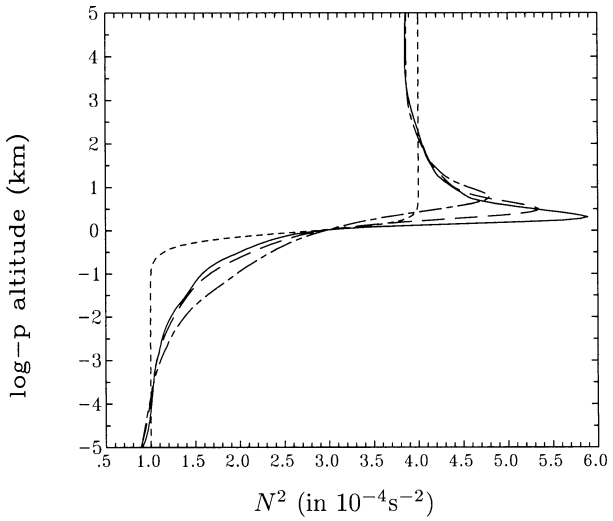

FIG. 14. Sensitivity with respect to δ, which measures the steepness of transition between the constant values N_t^2 and N_s^2 in the background atmosphere. The different profiles are composites of N^2 in the vortex center as function of z relative to the thermal tropopause. The model setup is identical to that in Fig. 12a expect that $\delta = 200$ m (solid line), $\delta = 400$ m (long dashes), and $\delta = 800$ m (long–short dashes). The short dashes depict $N_{\text{ref}}^2(z)$ for $\delta = 200$ m.

neither the observed sharpness of the peak nor the near discontinuity of N^2 across the tropopause are borne out very well. We did a sensitivity study repeating the computations shown in Fig. 12a for different values of δ, which is the transition scale between N_t^2 and N_s^2 defining the reference profile $N_{\text{ref}}^2(z)$. The result is shown in Fig. 14. Subsequently halving the value of δ from 800 m over 400 m to 200 m increases the maximum value of N^2 at the peak by about 0.5×10^{-4} s^{-2} each time. In addition, for the smaller values of δ the peak is located closer to the reference level (which is at $z = 0$ in Fig. 14). We conclude that in our model the characteristic features of the composite N^2 like the sharp increase across the tropopause and the peak just above the tropopause are the more pronounced the more N_{ref}^2 is characterized by a sharp transition across the tropopause.

The present study does not answer the question of what eventually determines the structure of static stability in the real atmosphere. In particular we did not address the question regarding the mechanism that produces a tropopause in the reference atmosphere; the near discontinuity in N_{ref}^2 across the tropopause was simply specified and turned out to be important in producing the peak in N^2 in the final profiles. We only considered one side of the coin focusing on the conservative generation of synoptic-scale anomalies and their effect on N^2. In the long run there must be competing nonconservative processes so as to establish a statistically stationary climatology. It is interesting in this context to note that there may be a pronounced asymmetry between cyclones and anticyclones regarding the dominant decay mechanism (cf. Wirth 1995; Zierl and Wirth 1997). A more complete model is needed to describe the competition between these different processes. Such a model should also produce a realistic spectrum of anomalies in a self-consistent manner, which is not possible with the current approach. Haynes et al. (2001) presented a study in which baroclinic life cycles compete against Newtonian relaxation toward a baroclinically unstable equilibrium state. It would be interesting to reanalyze the results from such a model using our findings as working hypotheses, and to test whether, or to what extent, our dynamical mechanisms can be identified and prove important in a climatological sense.

In the light of the above caveats and the idealized nature of our approach, the results should be viewed as suggestive. However, regarding the fact that our basic mechanism is related to fundamental properties of balanced flow and encouraged by the good qualitative agreement between our synthetic composites and corresponding observations, we conclude that nonlinear balanced dynamics is likely to play a role in producing the characteristic shape of the profile of static stability in the extratropical tropopause region, and especially in producing the sharp peak in N^2 right above the tropopause.

Acknowledgments. The author wants to thank T. Birner and two anonymous referees for constructive criticism.

REFERENCES

Andrews, D. G., J. R. Holton, and C. B. Leovy, 1987: *Middle Atmosphere Dynamics.* Academic Press, 489 pp.

Appenzeller, C., H. C. Davies, and W. A. Norton, 1996: Fragmentation of stratospheric intrusions. *J. Geophys. Res.,* **101,** 1435–1456.

Birner, T., A. Dörnbrack, and U. Schumann, 2002: How sharp is the tropopause at midlatitudes? *Geophys. Res. Lett.,* **29** (14), 1700, doi:10.1029/2002GL015142.

Bishop, C. H., and A. J. Thorpe, 1994: Potential vorticity and the electrostatics analogy: Quasi-geostrophic theory. *Quart. J. Roy. Meteor. Soc.,* **120,** 713–731.

Defant, F., and H. Taba, 1957: The threefold structure of the atmosphere and the characteristics of the tropopause. *Tellus,* **9,** 259–274.

Hakim, G. J., 2000: Climatology of coherent structures on the extratropical tropopause. *Mon. Wea. Rev.,* **128,** 385–406.

Haynes, P., J. Scinocca, and M. Greenslade, 2001: Formation and maintenance of the extratropical tropopause by baroclinic eddies. *Geophys. Res. Lett.,* **28,** 4179–4182.

Hoskins, B. J., M. E. McIntyre, and A. W. Robertson, 1985: On the use and significance of isentropic potential vorticity maps. *Quart. J. Roy. Meteor. Soc.,* **111,** 877–946.

Muraki, D. J., and G. J. Hakim, 2001: Balanced asymmetries of waves on the tropopause. *J. Atmos. Sci.,* **58,** 237–252.

Newton, C., and E. O. Holopainen, Eds., 1990: *Extratropical Cyclones: The Erik H. Palmén Memorial Volume.* Amer. Meteor. Soc., 262 pp.

Palmén, E., 1949: Origin and structure of high-level cyclones south of the maximum westerlies. *Tellus,* **1,** 22–31.

——, and C. W. Newton, 1969: *Atmospheric Circulation Systems.*

International Geophysics Series, Vol. 13, Academic Press, 603 pp.

Thorpe, A. J., 1985: Diagnosis of balanced vortex structure using potential vorticity. *J. Atmos. Sci.*, **42,** 397–406.

——, 1986: Synoptic scale disturbances with circular symmetry. *Mon. Wea. Rev.*, **114,** 1384–1389.

——, and C. H. Bishop, 1995: Potential vorticity and the electrostatics analogy: Ertel-Rossby formulation. *Quart. J. Roy. Meteor. Soc.*, **121,** 1477–1495.

Wirth, V., 1995: Diabatic heating in an axisymmetric cut-off cyclone and related stratosphere–troposphere exchange. *Quart. J. Roy. Meteor. Soc.*, **121,** 127–147.

——, 2000: Thermal versus dynamical tropopause in upper tropospheric balanced flow anomalies. *Quart. J. Roy. Meteor. Soc.*, **126,** 299–317.

——, 2001: Cyclone–anticyclone asymmetry concerning the height of the thermal and the dynamical tropopause. *J. Atmos. Sci.*, **58,** 26–37.

Zängl, G., and V. Wirth, 2002: Synoptic-scale variability of the polar and subpolar Tropopause: Data analysis and idealized PV inversions. *Quart. J. Roy. Meteor. Soc.*, **128,** 2301–2315.

Zierl, B., and V. Wirth, 1997: The influence of radiation on tropopause behaviour and stratosphere–troposphere exchange in an upper tropospheric anticyclone. *J. Geophys. Res.*, **102,** 23 883–23 894.